5B.3

SCALING PROPERTIES OF TEMPERATURE SPECTRA IN THE SURFACE FRICTION LAYER

Johannes Laubach[1,*] and Keith G. McNaughton[2, 3]

[1] Manaaki Whenua – Landcare Research, P.O. Box 40, Lincoln 7640, New Zealand

[2] School of GeoSciences, University of Edinburgh, Edinburgh EH9 3JU, Scotland

[3] Present address: 31 Paretu Drive, RD 1, Kerikeri 0294, New Zealand

ABSTRACT

Temperature variance and temperature power spectra have always presented a problem to the standard Monin-Obukhov similarity model. Recently that problem has intensified for convective boundary layers with the demonstration by Smedman et al. (2007, Q. J. Roy. Meteorol. Soc. 133: 37-51) that temperature spectra can have two distinct peaks in slightly unstable conditions, and by McNaughton et al. (2007, Nonlin. Proc. Geophys. 14: 257-271) who showed that the wavenumber of the peak of temperature spectra close above the surface friction layer (SFL) can be sensitive to the depth of the convective boundary layer, z_i. Neither the two-peak form at slight instability nor the dependence of peak position on z_i at large instability are compatible with the Monin-Obukhov model.

Here we examine the properties of temperature spectra from between these extremes, using observations made within unstable surface friction layers over grassland in the Coorong region of South Australia. During our observations the ABL depth, z_i, ranged from 126 to 1300 m, SFL depth, z_s, ranged from 18 to 290 m, and the ABL's convective structure parameter z_i/z_s ranged from 2.2 to 69. We base our analysis on the suggestion by McNaughton et al. (2007) that temperature transport through most of the SFL is by streamwise roll vortices formed by eddies from the outer inertial subrange interacting with the ground, with frictional turbulence being important only very near the ground ($z < 0.03\ z_s$).

The main results are: 1) There is an orderly succession in spectral shape, dependent on z/z_s: the T spectra have an increasingly sharp peak for z approaching z_s; conversely, the spectra become flatter and wider as z/z_s decreases. 2) The low-wavenumber range (production range), the peak region and the high-wavenumber range (inertial sub-range) each obey a different scaling, with different combinations of z, z_i and z_s involved. For z approaching z_s, the scaling expressions converge towards those found above the SFL by McNaughton et al. (2007). 3) The dependence of peak position on both z_i and z_s is consistent with the observations of Smedman et al. (2007). This includes the emergence of a second peak for certain combinations of the scaling parameters.

1. INTRODUCTION

The "Kansas" experiment (Kaimal et al. 1972) and the "Minnesota" experiment (Kaimal et al. 1976) have an established place in the history of micrometeorology. The results from these experiments, interpreted within the framework provided by the Monin-Obukhov and Deardorff similarity schemes, have become the standard description of the the atmospheric surface layer and mixed layers and, resting on this, the two similarity schemes are now the foundation on which almost all models of the atmospheric boundary layer (ABL) are built. Even so, the temperature spectra from the Kansas experiment were a direct challenge to the concepts that underlie the Monin-Obukhov theory. Thus Kaimal et al. (1972, p. 571 and Fig. 18) noted that as the Monin-Obukhov similarity variable ζ (= z/L, where z is height above ground and L is the Obukhov length) changed smoothly through dawn, the peak of the temperature spectrum moved discontinuously. In stable stratification around dawn, which is to say as $\zeta \rightarrow 0^+$ (where "0+" means approaching 0 from positive values), the peak moved smoothly to lower frequencies, but as ζ passed through zero to negative values, the peak's position jumped down by a decade. As the day progressed and conditions became more unstable, the peak moved smoothly back to higher frequencies, attaining intermediate values between those before and after the discontinuous morning transition. This behaviour is certainly counter-intuitive when placed in the context of a model whose underlying concept is of local eddies whose form and

* *Corresponding author address:* J. Laubach, Landcare Research, P.O. Box 40, Lincoln 7640, New Zealand, e-mail: LaubachJ@Landcareresearch.co.nz.

velocity scale depends on the local shear and buoyancy flux (Obukhov 1946), both of which change continuously. This behaviour was carefully recorded by Kaimal et al. (1972), but it received no further attention in the following 34 years. Recently two papers have described other features of temperature spectra from unstable conditions that also challenge the Monin-Obukhov/Deardorff interpretation of temperature spectra.

The first of these papers is by Smedman et al. (2007), henceforth SHHS07. They reported pre-multiplied temperature spectra, measured over both land and sea, with conditions ranging from slightly unstable with $L \approx -400$ m to moderately unstable with $L \approx -10$ m. In the range from $L \approx -150$ m to -40 m, they observed spectra with two distinct peaks, not just one as expected from the Kansas results (their Fig. 7). One of the two peaks was located at a scaled frequency $f \approx 0.2$ ($f = n\ z/u$ where n is observed frequency and u is mean wind speed at height z), a factor 3 or 4 higher than the peak at $\zeta = 0^+$ from Kansas (i.e. the peak at neutral stability approached from the stable side). The other peak was at about $f \approx 0.01$. As conditions became more unstable ($L \approx -10$ m) the latter peak shifted to higher frequencies. The peak at higher frequency meanwhile diminished in power while its frequency remained approximately constant so the lower-frequency peak came to dominate in moderately unstable conditions, with $\zeta \approx -1$. Similar behavior was noted in the w-T cospectra (where w stands for vertical windspeed and T for temperature). In the other direction, approaching neutral stratification from the unstable side, SHHS07 (Figs. 7 to 9) found that the lower-frequency peak disappeared and the peak at $f \approx 0.2$ became dominant.

Considering the results of SHHS07, it seems likely that Kaimal et al. (1972) described only the lower-frequency peak in their paper, explaining the jump through neutral and the regression of the peak position thereafter. SHHS07 propose a new transport mechanism to account for their results. This is developed within the context of the "impinging eddies" model of Hunt and Morrison (2000) and Högström et al. (2002). They propose that in the slightly unstable conditions heat is transported both by longitudinal rolls whose height spans the whole ABL and by smaller-scale eddies that impinge onto the surface and create smaller-scale turbulence.

The second paper challenging the Monin-Obukhov interpretation of T spectra is by McNaughton et al. (2007), henceforth MCM07. They reported spectra for very unstable conditions, with $L > -2$ m and $\zeta < -0.73$ at their lowest level, over a very smooth and extensive playa surface. MCM07 observed temperature spectra with single peaks like Kaimal et al. (1972) and SHHS07 for very unstable conditions, but unlike those authors, they needed to scale their wavenumber axis using the mixed length scale ($z_i^{1/2}\ z^{1/2}$) in order to collapse the spectral peaks, where z_i is the depth of the convective boundary layer (CBL). To collapse the large-wavenumber end of the spectra they needed to scale the wavenumber axis using ($z_i^{1/4}\ z^{3/4}$). The appearance of z_i in these scales is in direct contradiction to the Monin-Obukhov premise that only local parameters are needed to scale local processes. This unexpected appearance of mixed length scales means that we have to rethink the interpretation of the Kansas results, which were plotted against $n\ z/u$. It may be that the unresolved (stippled) region in Fig. 9 of Kaimal et al. (1972) is, at least in part, a product of incorrect scaling of their spectra.

The purpose of this paper is to introduce some of our own spectral observations made in conditions ranging from weakly to moderately unstable, and to interpret these new results and the results of Kaimal et al. (1972), SHHS07 and MCM07 using a structural model of convection in the CBL. In the next section we introduce this structural model, called here the "impinging-eddies model". Then we describe the new observations, show that they are compatible with the observations of previous workers quoted above, and finally argue how all of the observations can be explained by the new model.

2. THE IMPINGING-EDDIES MODEL

We will use the structural model of turbulence in the lower part of the CBL developed by McNaughton (2004a, b; 2006) and MCM07 to interpret temperature spectra. By "structural" we mean a model that describes turbulence in terms of the nature and forms of the coherent structures, their energies and their interactions. The model has two main parts, each of which has been developed somewhat separately in past publications, but here we use them together to explain scalar transport within the surface friction layer (SFL). We use the name "surface friction layer" to denote the layer of the atmosphere in contact with the ground in which the surface drag is an important scaling parameter for velocity spectra. The first part of the model chiefly concerns the momentum-transporting structures within the SFL (McNaughton 2004a, b; 2006). The second part of the model concerns the eddies observed above the SFL (MCM07).

Here we describe this model only to the extent needed to interpret temperature spectra, and add explanatory material not present in the other papers. The reader is referred to the original papers for the supporting arguments and the experimental evidence. We begin by describing the main kinds of coherent structures of the model, then go on to describe how these transport heat. The model proposes two main kinds of coherent structures, or eddies: outer and inner eddies.

2.1 *Outer Eddies*

The "outer" eddies are associated with top-down processes and outer scaling. They form in the main part of the CBL and have energies that depend on the turbulence energy budget of the whole CBL. Outer eddies include the large convective circulations that span the CBL, which might be cellular circulations or convective rolls according to the conditions (Etling and Brown 1993), together with the smaller eddies associated with the internal hand-down of energy from these large eddies to smaller and smaller ones as the energy passes down the outer inertial subrange towards dissipation. The turbulence processes associated with these outer eddies are top-down in the sense that they reflect processes active throughout the CBL, usually overhead for a ground-based observer, and in the sense that the flow of turbulence energy is unambiguously from larger to smaller-scale structures. We will be concerned with outer eddies principally when they are in contact with the ground, which is to say when they are "attached". A feature of their attachment is that the form of attached eddies depends systematically on height above ground, z, which can then appear in various scaling relationships. All but the largest of the attached eddies derive from the eddies of the outer inertial subrange impinging onto the ground. These take the form of elongated roll eddies under the action of blocking by the ground, wind shear and surface drag. Attached roll eddies transport scalars quite efficiently, as will be described below.

2.2 *Inner Eddies*

The "inner" eddies are associated with bottom-up turbulence processes and inner scaling. They form within the bottom-most part of the impinging outer eddies as they scrape along the ground. The main inner eddies are also attached and take the form of hairpin packets, though less-structured and detached inner eddies are formed also as the main eddies break down and their energy cascades down the inner inertial subrange. McNaughton (2004b) modeled the hairpin packets as "TEAL" (Theodorsen's ejection amplifyer-like) cascades, which are upscale sequences of ejections and hairpin vortices. These cascades are bottom-up in the sense that they originate at the ground and grow outwards into the flow. Collectively the TEAL structures form a complex system of interacting eddies that transfers momentum efficiently to the ground. The growth of individual TEAL structures relies on substantial pressure redistribution of energy and momentum, so scalars, which are not transported by pressure, get left behind. That is to say, the inner turbulence is not very efficient at transporting scalars.

2.3 *Energy Transfer From Outer To Inner Eddies*

The inner eddies take their energy from the impinging outer eddies which create them, so the energy transfer from the outer to the inner-scale eddies involves a spectral jump, from the larger scale of the outer roll eddies to the much smaller scale of the individual hairpin packets. Hunt and Carlotti (2001) call this "long range interaction or 'elevator-like' transfers", though the model they employ to explain it is very different to the one we present here. The significance of this cross-species transfer for us is that it not only drives the inner eddies, but saps the energy of the impinging outer eddies, which therefore have reduced lifetimes, particularly short if the inner eddies occupy more than a thin layer at their bottoms. We therefore expect the energy of the outer impinging eddies to decrease sharply when their heights are less than about a decade greater than the heights reached by the inner TEAL cascades. For that reason we expect the smallest outer roll eddies that are in contact with the ground to have diameters that are a small multiple of the depth of the SFL, z_s.

2.4 *Depth Of The Surface Friction Layer*

The depth of the SFL, z_s, is an important scaling parameter in our model. It is found by matching the power needed to maintain the upwards growth of the inner turbulence cascade stuctures with the power flowing down the outer Richardson cascade to eddies of similar size, which tends to distort and so terminate the growth of the inner cascades. Equating the two energy flows gives (MCM07):

$$z_s = u_\varepsilon^3/(k\,\varepsilon_o) \qquad (1)$$

where k is the von-Kármán constant and ε_o the dissipation rate in the bulk of the CBL, with subscript "o" meaning "outer" (outside the SFL). $u_\varepsilon = \left(u_*^3 + \overline{v_*^3}\right)^{1/3}$ is the "dissipation velocity". Here u_* is the friction velocity in the SFL and v_* its analogue for the fluctuating component of surface shear stress. $v_* > 0$ is caused by the unsteadiness of mean wind speed and direction that is always present in the ABL, but not in laboratory flows. In (1), both ε_o and u_ε create practical difficulties because they cannot easily be measured with standard instrumentation, like sonic anemometers in the SFL.

Firstly, to know u_ε we must know $\overline{v_*^3}$, and that would require a rapid-response drag plate at the ground for direct measurement. However, there are two options how u_ε can be estimated. The first is to ignore $\overline{v_*^3}$ and set $u_\varepsilon = u_*$. This will be a good approximation in a windy ABL, less so in a CBL with weak and variable winds. The alternative arises from u_ε being closely related to the profile of the dissipation rate within the SFL, $\varepsilon(z)$, via the relationship

$$u_\varepsilon = (k\,\varepsilon\,z)^{1/3}\,f(1) \tag{2}$$

where $f(1)$ stands for an unknown function of magnitude 1. Setting $f = 1$ gives thus an approximation for u_ε requiring knowledge of ε, which can be computed from the inertial subrange of the horizontal wind spectrum. The advantage of this method is that u_ε from (2) is less prone to random sampling error than u_* and not subject to flow distortion, while u_* is.

Secondly, to measure ε_o directly we would have to go above the SFL. When this is not possible, it can be estimated from a very rough turbulence energy budget for the CBL. This estimate sets buoyant production averaged over the height of the CBL equal to the average dissipation rate. The buoyant production of kinetic energy decreases linearly to zero at z_i (neglecting entrainment) so the average buoyant production of kinetic energy is about $g\,H_0/(2\,T)$, where g is acceleration due to gravity and $H_0 = \overline{w'T_v'}$ is the local turbulent virtual temperature flux ("buoyancy flux") originating from the underlying surface. The outer dissipation rate is uniform with height above the SFL (Kaimal et al. 1976). Equating these we have

$$\varepsilon_o \approx g\,H_0/(2\,T) \tag{3}$$

Inserting the approximations (2) and (3) into (1), z_s can be estimated as

$$z_s = 2\,T\,\varepsilon\,z\,/(g\,H_0) \tag{4}$$

provided that $z << z_s$.

Comparison of (4) to the definition of the Obukhov length,

$$L = -u_*^3\,T/(k\,g\,H_0) \tag{5}$$

reveals that under the condition that $u_* \approx (k\,\varepsilon\,z)^{1/3}$,

$$-z_s/L \approx 2 \tag{6}$$

The "≈" sign may mean ±50 %, but it gives a good order-of-magnitude relationship that is useful when comparing to published results where temperature spectra are ranked according to values of $|L|$.

2.5 *Heat Transport By Outer Eddies*

The outer eddies are the principal agent of scalar transport in the lower parts of CBLs, even down through most of the SFL. The impinging roll eddies form pairs or arrays aligned with the wind. They sweep scalars from the ground inwards towards, and then upwards within, the common-up regions between pairs of counter-rotating roll vortices. The heat plumes therefore appear as long thin sheets of rising warmed air. Puthenveettil and Arakeri (2005) call these sheet plumes. The process can work because pressure maintains the form of the roll vortices, and so the continuity of the material motion within them, by opposing the distorting effects of drag (Zhuang 1995). This continuity of motion over significant distances compared to z means that the roll vortices can transport scalars efficiently. Indeed, they carry the scalars so efficiently that the scalars' fluctuations display an outer-scale signature even at heights that are a small fraction of z_s (Kader and Yaglom 1990).

The inner-scale turbulence does, however, play an important role at small heights where the outer motions have very little energy and are very nearly horizontal. The inner turbulence carries the scalar upwards the first little distance from the ground, far enough to load it onto the "conveyor belt" provided by the outer eddies. Sequences of roll eddies of larger and larger scale then carry the scalars away. The outer eddies occur in a range of sizes, with larger eddies sweeping the sheet plumes together, forming larger and larger sheet plumes as height increases until these plumes merge to become the main thermals of the large-scale circulations in the CBLs. This occurs in an organized, top-down way so that the size of the sheet plumes reflects both the merging, which is related to the outer length scale, z_i, and the scale of the transporting roll eddies, which scale on z because they are attached. At heights greater than z_s the lengths of the thermal structures scale on the

mixed length scale ($z_i^{1/2}\ z^{1/2}$). This scaling is very clear in the observations of MCM07. At heights comparable to or smaller than z_s, the attached eddies do not scale on z any more, because interaction with the inner eddies destroys the smaller ones and sets a minimum outer-eddy size that is proportional to z_s (see Section 2.3). We thus predict that the lengths of the thermal structures within the SFL have a mixed length scale ($z_i^{1/2}\ z_s^{1/2}$).

2.6 *Translation Speed Of The Outer Eddies*

In order to convert from frequency n (observed with a fixed sampling rate) to wavenumber κ, the translation speed needs to be defined. While small eddies, in particular those from the inner inertial subrange, quite plausibly travel at the local windspeed $u(z)$, this cannot be expected for the outer eddies. The largest, CBL-spanning, eddies travel at the mean windspeed of the free CBL, u_m. This value is likely to be the upper limit for the translation speed of the heat-transporting eddies. Like ε_o, u_m is not available from measurements within the SFL. On the other hand, based on the notion that z_s sets the minimum size of the attached eddies, it is reasonable to suppose that $u_s = u(z_s)$ is a good approximation of their translation speed. Invoking (6), we estimate u_s as $u(-2\ L)$ by extrapolation from the windspeeds measured within the SFL, using the classical surface-layer wind profile for unstable stratification (Paulson 1970). Frequency is then converted to wavenumber by $\kappa = 2\ \pi\ n/u_s$, and κ is non-dimensionalised by multiplication with an appropriate length scale.

3. DATA COLLECTION AND PROCESSING

The dataset presented here was collected in an experiment whose original purpose was to investigate the structure of the ABL across a change in terrain roughness, to be reported elsewhere. It contains fewer runs than the data of SHHS07 or MCM07, but has the advantage that aircraft observations are available to determine z_i. The aircraft was an HK 36 TTC ECO-Dimona motorglider (Diamond Aircraft Industries, Wiener Neustadt, Austria) owned and operated by Airborne Research Australia – Flinders University, Adelaide, South Australia. It is permanently equipped with a "BAT" turbulence probe to measure pressure, all three components of airspeed and temperature at 20 Hz (Hacker and Crawford 1999), as well as all necessary equipment to take out aircraft motion and calculate the wind vector in ground coordinates.

3.1 *Experimental Site And Setup*

The experiment was conducted in October 2005. The site was 7 km inland from the Coorong coast of South Australia (35.9° S, 139.5° E). It was chosen because it featured a straight edge of a block of scrubland bordering on a paddock surface, with the edge running parallel to the coast (from NNW to SSE) and thus expected to be perpendicular to the predominant wind direction at daytime. Three sonic anemometers were set up on the paddocks. One of them was an 81000V (RM Young, Traverse City, Michigan), mounted on top of a telescope mast, 7.0 m above ground. The others were CSAT-3 (Campbell Scientific, Logan, Utah), mounted on separate poles at 2.5 m height. One of the CSAT-3 was horizontally 8 m away from the RM Young, close enough to investigate the height dependence of turbulence parameters over the paddock directly. The other CSAT-3 was 450 m away to the south, to assess if the slightly different vegetation there caused a difference in roughness. This was not found to be the case, so we can treat the measurements with the two CSAT-3 as duplicates in the cross-wind direction over the same surface. A second RM Young sonic was operated in the scrub, 500 m downwind of the edge, at 7.0 m above ground. Vegetation height in the scrub was about 2.5 m. The sonic over the scrub thus operated in the roughness sublayer, not in the SFL, and for that reason will not be considered here.

3.2 *Aircraft Data*

The task of the aircraft in this experiment was usually to fly grid patterns between 10 and 100 m height above the paddock and scrub, during the afternoon, in order to collect high-frequency wind and temperature data along and across the turbulent structures in the SFL. Because of this flight pattern, it was not possible to derive ε_o from aircraft data on a regular basis. For a handful of straight aircraft runs above the SFL, it was attempted to estimate ε_o from alongwind spectra. In about half of them, the ε_o estimates agreed well with results from (3), in the others, they were up to a magnitude larger. We concluded that the aircraft runs were not long enough to give meaningful statistics for this purpose.

The depth of the ABL was directly obtained twice per day, when the research aircraft measured vertical profiles of temperature and windspeed on arrival (descent) and on departure (ascent). z_i was then taken as the bottom level of the lowest strongly stable section in the profile of potential temperature. For the first four days of measurements, aircraft profiles were

either not reaching high enough or showed a complex ABL structure, so that the extent of the outer layer relevant for our scaling purposes was ambiguous. We therefore restrict analysis to the last four days, when z_i was either approximately constant between descent and ascent (13 Oct, 725 m) or grew at an average rate, taken linearly in time, that seemed plausible (25 m h^{-1} on 14 Oct, for an already deep CBL, or 63 m h^{-1} on 15 and 16 Oct, for the initially shallow ABL shortly after arrival of the sea breeze).

3.3 *Sonic Anemometer Data*

Data collection, with both sonic types, was operated at 20 Hz output. For the CSAT-3, an oversampling factor of 3 was used (i.e. internally, samples were taken at 60 Hz), to avoid aliasing. The oversampling error was then removed with the transfer function given by Horst and Oncley (2006). The RM Young 81000 V does not offer the option of oversampling at 20 Hz, but since it was operated at larger height (7.0 m), aliasing would have been smaller than for the CSAT-3 at 2.5 m and could be neglected.

Measurements were taken only on days when the research aircraft was available to operate, usually for between 2 and 6 hours in the afternoon. Collected data were restricted to wind directions between 164° and 339°. The fetch over uniform paddock surface was of order 3 km for these directions. Runs with positive stability parameter L (near dusk) were excluded. During eight days of measurement, there were 44 half-hour runs of acceptable wind direction when all sonics operated simultaneously. Of these, 25 were on the four days when z_i could be determined with confidence: 6 on 13/10, 10 on 14/10, 5 on 15/10 and 4 on 16/10.

Power spectra for the wind components and temperature were calculated with the wavelet algorithm of Grinsted et al. (2004), based on the Morlet wavelet. We compared the wavelet-based spectra to spectra based on traditional Fourier transform and found the former slightly smoother than the latter but without any systematic differences. The horizontal wind spectra were used to calculate ε and, using (2), u_ε. The temperature flux at 2.5 m was used as H_0 in (3) and (4), neglecting the small difference between acoustic temperature and virtual temperature, in order to calculate ε_o and z_s. Scaling of the T spectra was done for each run individually, on both measured and modelled spectra. Scaled spectra were then averaged into five classes according to z_s and z_i.

The two sonic types were compared in a separate experiment. Each sonic was set up on its own mast, 5.5 m apart in a straight line, 3.88 m above a flat paddock with an upwind fetch of 600 m to the nearest hedge. In this comparison experiment, running for 3 days (daytime only), the standard deviation of T differed by 3 % between CSAT-3 and RM Young, and by 1 % between sonics of the same type. Vertical temperature fluxes differed by 4 % between types and 2 % between identical sonics, respectively. u_* typically differed by 3 % on average for any pair, but with much larger scatter than for σ_T and $\overline{w'T'}$, while u_ε differed only by 1 % on average, for any pair, with very little scatter. Power spectra and cospectra were also compared and did not indicate any systematic differences between CSAT-3 and RM Young.

4. RESULTS AND DISCUSSION

4.1 *ABL Development And Scaling Parameters*

During our observations the ABL depth, z_i, ranged from 126 to 1300 m, SFL depth, z_s, ranged from 18 to 290 m, and the ABL's convective structure parameter z_i/z_s ranged from 2.2 to 69. Table 1 shows how the 25 valid runs were grouped, and gives means and standard deviations of the scaling parameters z_s, z_i and u_s. The primary parameter for class selection is SFL depth: neighbouring classes differ by about a factor 2 to 3, except for Classes B and C, which cover the same range for z_s. These two classes, however, have very different ABL depth, which therefore acts as the secondary sorting parameter.

We describe briefly the ABL development underlying these data. On 13 Oct, the outer layer was represented by a well-mixed ABL, with neutral potential temperature profile. This ABL was capped at 725 m by a well-defined strong inversion. Windspeeds within it were high, with u_s > 11 m s^{-1}, and consequently, stratification was nearer to neutral than on the other days. Wind direction was steady around 240°. This day provided the runs of Class E (Table 1).

On 14 Oct, wind direction was steady too, at 220 (±10)°, but windspeeds were much lower, with $u_s \approx 3$ m s^{-1} until 13:00, then steadily increasing to about 6 m s^{-1}. When the aircraft arrived at 10:50, a CBL had already developed up to 1190 m. By 13:00, this CBL had grown to 1245 m and heated up by about 1 K on average, due to entrainment of the warmer air aloft. In the upper half of the CBL the potential temperature profile was slightly stable, with a gradient of 0.6 * 10^{-3} K m^{-1} at 10:50 and 1.4 * 10^{-3} K m^{-1} at 13:00; in the lower half the profile was neutral. Stratification in the

Class	No. Runs	z_s (m)	z_i (m)	z_i / z_s	u_s (m s^{-1})	Comments
A	6	23 (4)	1226 (30)	55 (11)	3.5 (0.4)	deep CBL
B	4	38 (7)	1273 (33)	35 (6)	5.2 (1.1)	deep CBL
C	4	39 (10)	200 (35)	5.4 (1.6)	5.8 (0.7)	developing sea breeze
D	5	69 (17)	277 (91)	4.0 (1.1)	6.7 (0.2)	developing sea breeze
E	6	227 (38)	725	3.3 (0.5)	12.1 (0.5)	steady breeze

Table 1 Classification of runs, primarily according to SFL depth, z_s, and secondarily, between Classes B and C, according to ABL depth, z_i. u_s is the mean translation speed of eddy structures, assumed as $u(z_s)$. For each class, means and standard deviations (in parentheses) of the parameter values are shown, except for z_i in Class E, which was assumed constant.

surface layer was moderately to strongly unstable: $-L$ < 25 m, hence according to (6), z_s < 50 m. This day provided the runs of Classes A and B.

By contrast, on 15 and 16 Oct the ABL was represented by a shallow sea breeze, the sudden arrival of which was documented by the sonic anemometer measurements on both days. On 15 Oct, the sea breeze arrived at the S paddock mast at 13:32 and at the scrub mast at 13:46. From the aircraft sounding at 14:00, its depth was obtained as 222 m, indicated both by a sudden increase in potential temperature and a reversal of wind direction, due to the offshore return flow which overlied the sea breeze. At the end of this day, the aircraft did not fly an ascent high enough to determine ABL depth, which was therefore estimated on the assumption that the ABL growth rate of 16 Oct also applied on 15 Oct. On 16 Oct, the depth of the sea breeze layer grew from 80 m at 12:00 to 215 m at 14:10. The ABL was thus shallower than on 15 Oct and the sea breeze arrived earlier, both because the angle between wind direction and orientation of the coastline was larger on 16 Oct than it was on 15 Oct (wind direction was around 180° on 15 Oct and around 210° on 16 Oct). Despite the difference in wind direction, we assume the same growth rate on both days because upwind land-use was similar, and the observed temperatures and windspeeds were similar for both days, too. Values for windspeed and z_s on these two days were intermediate between those of 13 and 14 Oct. Sorting by z_s, one run of 15 Oct and three of 16 Oct form Class C, and four runs of 15 Oct and one of 16 Oct form Class D.

Table 1 also shows the ratio z_i/z_s. For Classes A and B, z_i/z_s > 30. According to Etling and Brown (1993), a ratio $-z_i/L$ > 25 (with (6), roughly equivalent to z_i/z_s > 12.5) characterises a CBL that is dominated by large cellular structures. By contrast, for Classes C, D and E, z_i/z_s ranges from about 3 to 7 (hence $-z_i/L$ from about 6 to 14). Following Etling and Brown (1993), such values characterise a ABL in which pairwise longitudinal roll vortices are the dominant structures, and for even smaller $-z_i/L$ they are the only outer eddies that can exist. Another way of describing this situation, following our model, is that the SFL then fills the ABL completely.

4.2 *Comparing T Spectra To The Kansas Model*

The established set of model spectra in the surface layer are the "Kansas spectra" (Kaimal et al. 1972). These authors state that: "With appropriate normalization, the spectra and cospectra are each reduced to a family of curves which spread out according to z/L at low frequencies but converge to a single universal curve in the inertial subrange." The expectation that spectral shape varies only with stability is based on Monin-Obukhov similarity theory. However, in the unstable surface layer, the cited statement was never quite true. While the scaled spectra fell inside a range bounded by two curves, empirically determined by Kaimal et al. (1972), within that range they did not vary with z/L in a predictable fashion. For longitudinal and lateral wind spectra, that variation has been explained as a signature of large ABL-spanning eddies, and successfully modelled by adding z_i to the list of required parameters (Højstrup 1981). For temperature spectra, such an understanding of the variability in unstable stratification has been lacking.

Nevertheless, we begin our scaling attempts using the Kansas scheme (Figs. 1 and 2). For each class (Table 1) the spectra are first scaled individually then averaged to give the spectra shown. The fre-

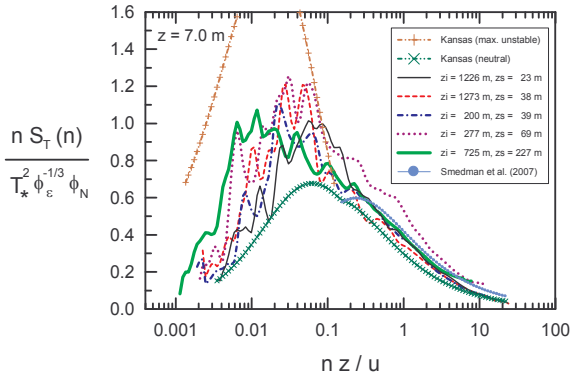

Figure 1. Temperature spectra at 7.0 m height, scaled in traditional fashion with stability-dependent scaling factors on the amplitude axis and local windspeed on the frequency axis. The spectra are averaged separately for the five classes defined in Table 1 (A: black, B: red, C: dark blue, D: purple, E: bright green). Also shown are the neutral (0+) Kansas spectrum (dark green with x symbols), the upper limit of the unstable range found at Kansas (Kaimal et al. 1972, brown with + symbols), and the "unstable very close to neutral" spectrum of Smedman et al. (2007) for $n\,z/u > 0.15$ (light blue with dots).

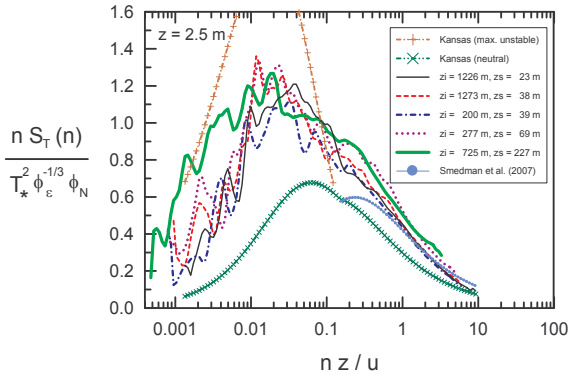

Figure 2. Same as Figure 1 but at 2.5 m height.

---

quency axis is scaled with measurement height as the length scale and local windspeed at that height as the velocity scale. On the amplitude axis, we include, like Kaimal et al. (1972), the factor $\varphi_N\ \varphi_\varepsilon^{-1/3}$ where $\varphi_\varepsilon = (u_\varepsilon/u^*)^3$. Assuming balance between dissipation and production, the dimensionless dissipation of temperature variance, φ_N, is substituted by the dimensionless temperature gradient, φ_h, using the best-fit expression of Högström (1988, Eq. 15). SHHS07 followed the same practice.

The following features are observed in Figs. 1 and 2. First, at low frequencies and in the peak region, the measured spectra fall between the curves marked as "Kansas (neutral)" and "Kansas (max. unstable)". Thus, our dataset is compatible with the data of Kaimal et al. (1972). Second, the class with the largest z_s (E) displays the lowest, and the class with the smallest z_s (A) displays the highest peak frequency, in line with the behaviour observed by Kaimal et al. (1972) that was referred to in the Introduction. Third, in the inertial subrange the measured spectra collapse well with each other at each height (except Class D at 7.0 m), however, they do not collapse between the two heights, and not with the neutral Kansas model curve, either. As a consequence of collapse in the inertial subrange and spread at low frequencies, there is an orderly succession in spectral shape, dependent on z/z_s: the T spectra have an increasingly sharp peak for z approaching z_s; conversely, the spectra become flatter and wider as z/z_s decreases.

For large frequencies, all the measured spectra converge towards the spectrum observed by SHHS07 (their Figs. 8 and 9) for "unstable very close to neutral" stratification (indicated with thick dots in Figs. 1 and 2). This curve is similar to the inertial-subrange part of the neutral Kansas spectrum, but at about twice the normalised frequency. It appears that this curve represents a universal limit which is not accurately fitted by the Kansas model. The high-frequency part of the spectrum represents the action of the small-scale inner eddies. The convergence of all curves in this part of the spectrum indicates that inner eddies are – at least approximately – scaled correctly by the traditional scaling scheme; however, at low frequencies and in the peak region, where we expect outer eddies to be the main agents of transport, the traditional scaling scheme is unable to provide a universal description of the T spectrum.

4.3 *Scaling T Spectra With The Impinging-Eddies Model*

Alternatively, in Figs. 3 and 4 the T spectra are scaled according to the prediction of the impinging-eddies model. On the amplitude axis, we find empirically that good collapse of peak heights is achieved with a scaling factor $(z^{1/2}\ z_s^{1/2})^{2/3}\ \varepsilon_o^{2/3}/\overline{w'T'}^2$. This factor makes sense because it describes outer eddies of height scale z_s being blocked by the ground. The blocking is responsible for the dependence on z. At the top of the SFL, the blocking effect disappears. Above the SFL, because z_s is no longer limiting the

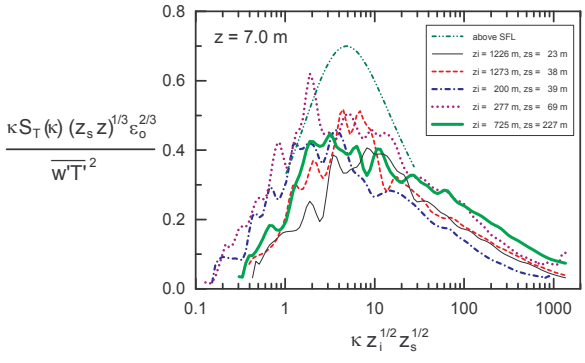

Figure 3. Temperature spectra at 7.0 m height, scaled according to the impinging-eddies model, with mixed length scales including SFL depth on both axes. The spectra are averaged separately for the five classes defined in Table 1 (A: black, B: red, C: blue, D: purple, E: bright green). Also shown is the peak region of the spectrum above the surface friction layer, as observed by McNaughton et al. (2007), with z replacing z_s on both axes (dark green).

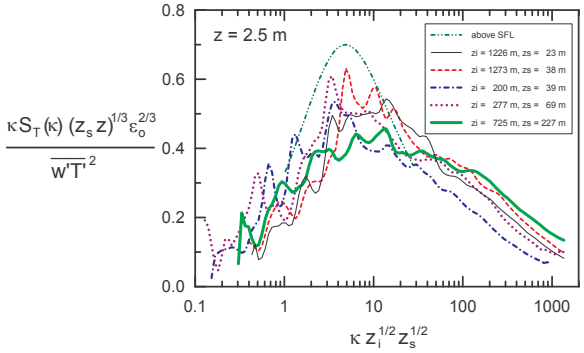

Figure 4. Same as Figure 3 but at 2.5 m height.

---

size of the most effective eddies, z_s is replaced by z, giving the scaling factor found by MCM07. The peak region of the spectrum above the SFL, following MCM07, is also shown in Figs. 3 and 4, with z replacing z_s on both axes. The peak amplitude of this curve is about 40 % larger than that of the spectra in the SFL (0.7 vs. 0.5), which suggests that the handover of the amplitude length scale is not exactly at $z = z_s$ but rather at $z \approx 3\ z_s$.

On the wavenumber axis, the expected length scale is $(z_i^{1/2}\ z_s^{1/2})$, see Section 2.5. Figs. 3 and 4 show that this scale is only partly successful in collapsing the peak positions of the spectra. For the two classes with large z_i/z_s (A and B, thin solid and dashed in the figures, respectively) the scaled peak wavenumbers are similar, and agree within 50 % with the "above SFL" curve. These two classes represent deep CBLs with cellular convection. However, for the three classes with $z_i/z_s < 8$ (C to E, dash-dotted, dotted, and thick solid, respectively), the scaled peak wavenumbers are a factor 2 to 3 smaller. These three classes represent shallower ABLs where the largest eddies are streamwise roll vortices (Etling and Brown 1993).

The factor 2 to 3 suggests that good collapse can be achieved if z_s is replaced by z_i, in other words, if the mixed length scale is substituted by the purely outer length scale z_i. In the context of the impinging-eddies model, this substitution can be explained as follows. Note that eddies scaling on z_s are really eddies larger than z_s (perhaps by a factor 3 as indicated by the amplitude scaling) or they would lose energy too fast. If z_i/z_s is less than a magnitude larger than 1, then the SFL occupies a substantial part of the ABL and the z_s-scale eddies are of a size close to z_i. In effect, the impinging eddies and the largest ABL structures become the same eddies. Therefore, the z_s scale must have a cap at some fraction of z_i, at which height the mixed length scale $(z_i^{1/2}\ z_s^{1/2})$ becomes indistinguishable from z_i, and there can be no larger roll eddies.

We can unify the qualitatively different results for cell-dominated CBLs and roll-dominated shallow ABLs by introducing x_e as the regime-dependent eddy-size length scale. On the wavenumber axis, x_e then combines with z_i, which describes the spacing rather than the size of the heat-carrying eddies, to the mixed length scale $(z_i^{1/2}\ x_e^{1/2})$. In a roll-dominated shallow ABL, $x_e = z_i$, in a cell-dominated CBL, $x_e = z_s$ within the SFL and $x_e = 2\ z$ above the SFL. By introducing the factor 2 in the latter we shift MCM07's curve (as in Figs. 3 and 4) upwards by $2^{1/2}$ in order to achieve the best match with the present data. This factor is plausible because the most effective eddies observed at a given height are those that have their centre at z, and thus reach twice as high.

This unified scaling is applied in Figs. 5 and 6. At 7.0 m (Fig. 5), the peak wavelengths collapse excellently. The peak amplitudes from the present experiment are all within 0.47 (±0.07), without any systematic order by class. The observed 15 % variation may well be due to the combined errors of the scaling variables ε_o, z_s and $\overline{w'T'}$. At 2.5 m (Fig. 6), Classes A to D show equally excellent collapse of the peak wavelength. Their amplitudes also agree well, within 0.56 (±0.06). This is somewhat larger than at 7.0 m, yet closer to the value of 0.7 found above the

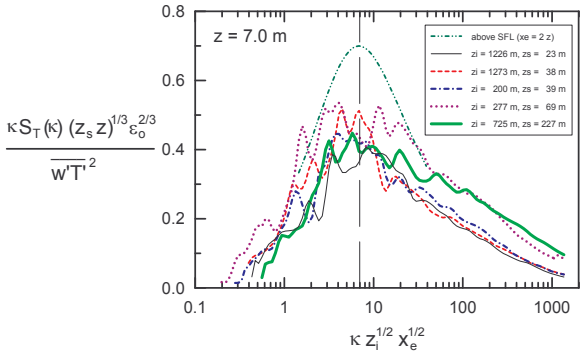

Figure 5. Temperature spectra at 7.0 m height, with revised scaling according to the impinging-eddies model: for $z_i/z_s > 8$, the eddy length scale x_e on the abscissa equals z_s (Classes A and B, black and red), for $z_i/z_s < 8$, $x_e = z_i$ (Classes C to E, blue, purple and bright green). Also shown is the peak region of the spectrum above the surface friction layer, as observed by McNaughton et al. (2007), assuming $x_e = 2\,z$ (dark green). The peak location is emphasized by a vertical dashed line.

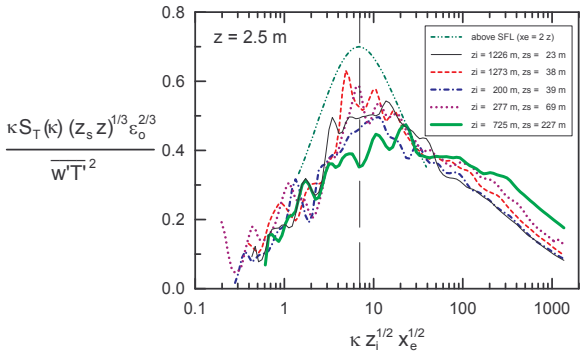

Figure 6. Same as Figure 5 but at 2.5 m height.

SFL. The class with largest z_s (E) exhibits the peak at smaller amplitude and larger wavenumber than the others, which we discuss further below.

Not only does the scaling in Fig. 6 collapse the peak regions reasonably well, it also collapses the spectra of all five classes excellently at small wavenumbers, for $\kappa\,(z_i^{1/2}\,x_e^{1/2}) < 3$. This gives strong support to the central assumption of our model that outer eddies are responsible for most of the scalar transport, and also to the notion that they need to be scaled as "blocked" eddies.

By contrast, at large wavenumbers, for $\kappa\,(z_i^{1/2}\,x_e^{1/2}) > 30$, the spectra diverge systematically, with the amplitude increasing for increasing z_s. Clearly, the impinging-eddies model cannot scale the spectrum at large wavenumbers correctly. We conclude that the low-wavenumber range (production range), the peak region and the high-wavenumber range (inertial subrange) each obey a different scaling, with different combinations of z, z_i and z_s involved, dependent not only on wavenumber range but also on the regime type as described above.

The spectrum of Class E at 2.5 m is the only one with $z/z_s < 0.03$. It falls into the "unstable very close to neutral" range for which SHHS07, using traditional scaling, observed the emergence of a well-defined high-frequency peak. Comparing the shape of this spectrum to the others in Fig. 6, it appears as if spectral energy has been systematically shifted away from the peak region (where the spectral shape appears almost "beheaded") to the high-wavenumber range (inertial subrange), where a secondary peak just begins to emerge. This behaviour is consistent with SHHS07's Fig. 7, where the amplitude at high frequencies increases systematically with increasing $|L|$. It is also consistent with our understanding of the interaction between outer and inner eddies (see Section 2.3): for $z/z_s < 0.03$, outer eddies are so much affected by destructive friction that they become less efficient than the inner eddies.

5. CONCLUSIONS

We have developed a new scaling scheme for the power spectrum of temperature in the surface friction layer. The scheme is based on the structural model of McNaughton (2006) and MCM07 in which impinging outer eddies, shaped as longitudinal roll vortices, are the main agents of scalar transport.

The new scheme successfully collapses the low-frequency regions and the peak regions of the T spectra in the SFL, for $z/z_s > 0.03$. The peak amplitudes scale on $(z^{1/2}\,z_s^{1/2})^{2/3}\,\varepsilon_o^{2/3}/\overline{w'T'}^2$, where the mixed z-z_s length scale describes eddies of height z_s being blocked by the ground. The wavenumber scales on a mixed length scale, too, with equal weight for ABL depth and horizontal eddy size x_e. The parameter x_e depends on the structure of the whole flow: it is equal to z_s within a SFL that occupies only the bottom part of a deep cell-dominated CBL, and to z_i in a SFL that fills most or all of a roll-dominated ABL. The same wavenumber scaling scheme is valid in a deep CBL above the SFL (MCM07) if x_e is identified with $2\,z$.

Frictional (inner) eddies become efficient only for $z/z_s < 0.03$, apparent by the emergence of a separate peak at high wavenumbers. However, even for

z/z_s > 0.03, frictional eddies affect the scaling of the high-wavenumber region of the spectrum, where the impinging-eddies model is not successful in collapsing the data. We conclude that no single scaling scheme works for all wavenumbers.

6. REFERENCES

Etling D, Brown RA (1993) Roll vortices in the planetary boundary layer: A review. Boundary-Layer Meteorol 65:215-248

Grinsted A, Moore JC, Jevrejeva S (2004) Application of the cross wavelet transform and wavelet coherence to geophysical time series. Nonlin Processes Geophys 11:561-566

Hacker JM, Crawford TL (1999) The BAT-probe: The ultimate tool to measure turbulence from any kind of aircraft (or sailplane). J Tech Soaring XXIII(2): 43-46

Högström U (1988) Non-dimensional wind and temperature profiles in the atmospheric surface layer: A re-evaluation. Boundary-Layer Meteorol 42:55-78

Högström U, Hunt JCR, Smedman A-S (2002) Theory and measurements for turbulence spectra and variances in the atmospheric neutral surface layer. Boundary-Layer Meteorol 103:101-124

Højstrup J (1981) A simple model for the adjustment of velocity spectra in unstable conditions downstream of an abrupt change in roughness and heat flux. Boundary-Layer Meteorol 21:341-356

Horst TW, Oncley SP (2006) Corrections to inertial-range power spectra measured by CSAT3 and Solent sonic anemometers, 1. Path-averaging errors. Boundary-Layer Meteorol 119:375–395

Hunt JCR, Carlotti P (2001) Statistical structure at the wall of the high Reynolds number turbulent boundary layer. Flow Turb Combust 66:453-475

Hunt JCR, Morrison JF (2000) Eddy structure in turbulent boundary layers. Eur J Mech B – Fluids 19:673-694

Kader BA, Yaglom AM (1990) Mean fields and fluctuation moments in unstably stratified turbulent boundary layers. J Fluid Mech 212:637-662

Kaimal JC, Wyngaard JC, Izumi Y, Coté OR (1972) Spectral characteristics of surface-layer turbulence. Quart J Roy Meteorol Soc 98:563-589

Kaimal JC, Wyngaard JC, Haugen DA, Coté OR, Izumi Y, Caughey SJ, Readings CJ (1976) Turbulence structure in the convective boundary layer. J Atmos Sci 33:2152-2169.

McNaughton KG (2004a) Attached eddies and production spectra in the atmospheric logarithmic layer. Boundary-Layer Meteorol 111:1-18

McNaughton KG (2004b) Turbulence structure of the unstable atmospheric surface layer and transition to the outer layer. Boundary-Layer Meteorol 112:199-221

McNaughton KG (2006) On the kinetic energy budget of the unstable atmospheric surface layer. Boundary-Layer Meteorol 118:83-107

McNaughton KG, Clement RJ, Moncrieff JB (2007) Scaling properties of velocity and temperature spectra above the surface friction layer in a convective atmospheric boundary layer. Nonlin Processes Geophys 14:257-271

Obukhov AM (1946) English translation 1971: Turbulence in an atmosphere with a non-uniform temperature. Boundary-Layer Meteorol 2:7-29

Paulson CA (1970) The mathematical representation of wind speed and temperature in the unstable atmospheric surface layer. J Appl. Meteorol. 9:857-861

Puthenveettil BA, Arakeri JH (2005) Plume structure in high- Rayleigh-number convection. J Fluid Mech 542:217-249

Smedman A-S, Högström U, Hunt JCR, Sahlée E (2007) Heat/mass transfer in the slightly unstable atmospheric surface layer. Quart J R Meteorol Soc 133:37-51

Wyngaard JC, Coté OR, Izumi Y (1971) Local free convection, similarity, and the budgets of shear stress and heat flux. J Atmos Sci 28:1171-1182

Zhuang Y (1995) Dynamics and energetics of convective plumes in the atmospheric surface layer. J Atmos Sci 52:1712-1722

Acknowledgements. This work was funded by the Marsden Fund of the Royal Society of New Zealand. We thank Jörg Hacker of Airborne Research Australia – Flinders University for operating the aircraft and processing the aircraft data. Tony McSeveny helped with setting up of the ground-based measurements. Hort Research (Kerikeri, New Zealand) and John Wilson (University of Alberta, Edmonton, Canada) each lent us a CSAT-3 sonic anemometer. We are grateful to the Birks family to allow this experiment being conducted on their land.